BAMS Article

Comprehensive Radar Data for the Contiguous United States

Multi-Year Reanalysis of Remotely Sensed Storms

Skylar S. Williams, Kiel L. Ortega, Travis M. Smith, and Anthony E. Reinhart

ABSTRACT: The Multi-Year Reanalysis of Remotely Sensed Storms (MYRORSS) dataset blends radar data from the WSR-88D network and Near-Storm Environmental (NSE) model analyses using the Multi-Radar Multi-Sensor (MRMS) framework. The MYRORSS dataset uses the WSR-88D archive starting in 1998–2011, processing all valid single-radar volumes to produce a seamless three-dimensional reflectivity volume over the entire contiguous United States with an approximate 5-min update frequency. The three-dimensional grid has an approximate 1 km × 1 km horizontal dimension and is on a stretched vertical grid that extends to 20 km MSL with a maximal vertical spacing of 1 km. Several reflectivity-derived, severe-storm-related products are also produced, which leverage the ability to merge the MRMS and NSE data. Two Doppler velocity-derived azimuthal shear layer maximum products are produced at a higher horizontal resolution of approximately 0.5 km × 0.5 km. The initial period of record for the dataset is 1998–2011. The dataset underwent intensive manual quality control to ensure that all available and valid data were included while excluding highly problematic radar volumes that were a negligible percentage of the overall dataset, but which caused large data errors in some cases. This dataset has applications toward radar-based climatologies, postevent analysis, machine learning applications, model verification, and warning improvements. Details of the manual quality control process are included and examples of some of these applications are presented.

KEYWORDS: Convective storms; Data mining; Data processing/distribution; Databases; Radars/Radar observations

https://doi.org/10.1175/BAMS-D-20-0316.1

Corresponding author: Kiel L. Ortega, kiel.ortega@noaa.gov

In final form 23 November 2021

AFFILIATIONS: Williams, Ortega, and Smith—Cooperative Institute for Severe and High-Impact Weather Research and Operations, University of Oklahoma, and NOAA/OAR National Severe Storms Laboratory, Norman, Oklahoma; **Reinhart**—NOAA/OAR National Severe Storms Laboratory, Norman, Oklahoma

The Multi-Radar Multi-Sensor (MRMS; Lakshmanan et al. 2007a; Smith et al. 2016; Zhang et al. 2016) system was made operational in the National Weather Service (NWS) in 2014. A key component of the MRMS system is software to merge individual radars together into a seamless latitude–longitude–height grid (Lakshmanan et al. 2006). The MRMS data can also be combined with other data, such as Near-Storm Environment (NSE) information provided by model analysis grids, to derive further products or analyses. While the operational MRMS system can provide an archive of data, any data delivery failures or delays, incorrect configurations, or computer downtime affect the overall completeness and accuracy of any operational archive. Thus, processing data in a reanalysis framework is necessary to provide a dataset that has been vetted for completeness and accuracy. The Multi-Year Reanalysis of Remotely Sensed Storms (MYRORSS) is that effort and is working to not only complete the base data of merged radar reflectivity data, but also derive further datasets that may be more approachable by users who may not have access to large computing resources.

Currently MYRORSS has processed data over 13 years spanning from 22 April 1998 through 31 December 2011 using the Warning Decision Support System–Integrated Information (WDSS-II; Lakshmanan et al. 2007a) suite of algorithms that is also used to create the operational MRMS products. The MYRORSS dataset benefits from data quality checks that included manual intervention for poor single-radar data quality and specific deletion of poor data volumes that caused severe errors in the resulting three-dimensional merged grid (see the "Additional quality control and known issues" section for specific examples of poor data quality). These additional quality control checks allow users to create more accurate analyses. The size of the dataset, combined with the data quality, lends this dataset to more complex applications such as machine learning. Other potential applications of the dataset include postevent analysis, radar climatologies, and hazardous weather event probabilities.

Data

The foundation for MYRORSS is from the Next-Generation Radar (NEXRAD) network composed of the WSR-88D systems. The Level II data from the WSR-88Ds, which contain reflectivity, mean radial velocity, and spectrum width, were accessed from the National Centers for Environmental Information (NCEI) and Amazon Web Services (AWS; NOAA/NWS/ROC 1991; Ansari et al. 2018). The average number of radars available in the NEXRAD Level II archive increases as years become more contemporary. In 1998, there were on average 76 radars available in the archive across the CONUS while at the end of 2011 there were on average 134 radars in the archive. During the timespan of the current MYRORSS dataset, the NEXRAD network was upgraded to a higher resolution and several new volume coverage patterns (VCPs) were implemented. Lower-resolution single-radar (hereafter "legacy") data have a spatial resolution of 1° azimuthal × 1 km range gate to a range of 460 km for reflectivity with velocity and spectrum width having a range to 230 km with a 250-m range gate. Higher-resolution single-radar (hereafter "superres") data have 0.5° azimuthal × 250 m range gate resolution to a range of 460 km for reflectivity and 300 km for velocity and spectrum width (Torres and

Curtis 2007). The WSR-88D network also began an upgrade to polarimetric capabilities starting in 2010 which was completed in 2013; however, the initial MYRORSS dataset uses only horizontal reflectivity, spectrum width, and Doppler velocity.

The MRMS reflectivity data were combined with NSE model analyses from the Rapid Update Cycle (RUC; Benjamin et al. 2004) to produce a variety of products, such as maximum expected size of hail (MESH; Witt et al. 1998), that may be used in the analysis of severe weather events. During the MYRORSS analysis period, the RUC model was upgraded to have improved spatial resolution. Before 2002, the RUC 40 km was used, while the 20-km analyses were used for the remainder of the processed period with occasional 13-km analyses used to gap-fill any missing 20-km analyses in the CIWRO/NSSL archive.[1]

[1] CIWRO/NSSL maintained an internal archive of RUC hourly analyses and used whatever highest resolution was available in the archive.

Methods

Data processing. Data processing began with single radar handling and was completed using the WDSS-II suite of algorithms (Fig. 1, see single radar processing). The first step was to convert the data files to Network Common Data Form (netCDF; Rew et al. 2015) from the binary format specified by the Radar Operations Center (NOAA NWS ROC 1991). Once the data were in netCDF format, a quality control neural network (Lakshmanan et al. 2007b) was used to remove nonmeteorological reflectivity features within the data such as biological targets and ground clutter. To help remove the biological clutter, but not snow since they can have similar appearances in the reflectivity field, the RUC surface temperature was used within the algorithm to determine whether snow was possible or not when quality controlling lower reflectivity values near the radar. An additional quality control algorithm was used to remove any additional radar "blooms," caused by biological scatter, around the radar site (Lakshmanan et al. 2010; Tang et al. 2011) that could make it past the initial quality control neural network.

Using the wind profile derived from RUC analyses for each radar site, radial velocity data were dealiased using methods developed by Jing and Wiener (1993) and expanded upon since by the Radar Operations Center (ROC).[2] Once dealiasing was completed, azimuthal shear was calculated using a linear least squares derivative to compute the rotational component of the radial velocity field (Mahalik et al. 2019). Azimuthal shear data within a 5-km range of the radar were not processed to reduce noise from ground clutter. Azimuthal shear was filtered using a reflectivity threshold of 40 dBZ and the reflectivity data were dilated prior to filtering. The dilation was performed using a 5×5 pixel neighborhood. In order for a new value to be placed in the center pixel, the neighborhood had to be at least 33% filled and the second largest value in the neighborhood was used as the new reflectivity value. Dilating the reflectivity allows for circulations along reflectivity gradients occurring at or near the edges of observed reflectivity to be properly maintained. Maximal azimuthal shear was calculated within two vertical layers: 0–3 km above ground level (AGL) to capture low-level rotation near the surface, and 3–6 km AGL to capture midlevel rotation within the storm.

[2] The dealiasing used for MYRORSS was from the Open Radar Products Generator 18 provided by the ROC. The code has been implemented in WDSS-II in the dealiasVel program. The dealiasVel program is updated with the latest code from the ROC, thus the latest versions of WDSS-II will not have the version of the dealiasing code used in MYRORSS processing.

Once single-radar processing was completed for all radars for a given day, the data were blended together using the radar data merging technique developed by Lakshmanan et al. (2006). These mosaics used the closest four radars available within 400 km to the given point within the domain. To reduce the time needed for merger calculations, the closest four radars were predetermined and hardcoded into a cache. For instance, say a cluster of five radars are close to a point, only the nearest four would be considered and the fifth was never used, even if one of the nearest four were unavailable. The merged data were blended such that contributions from the radars are weighted by the inverse square of the distance to the radar from each pixel.

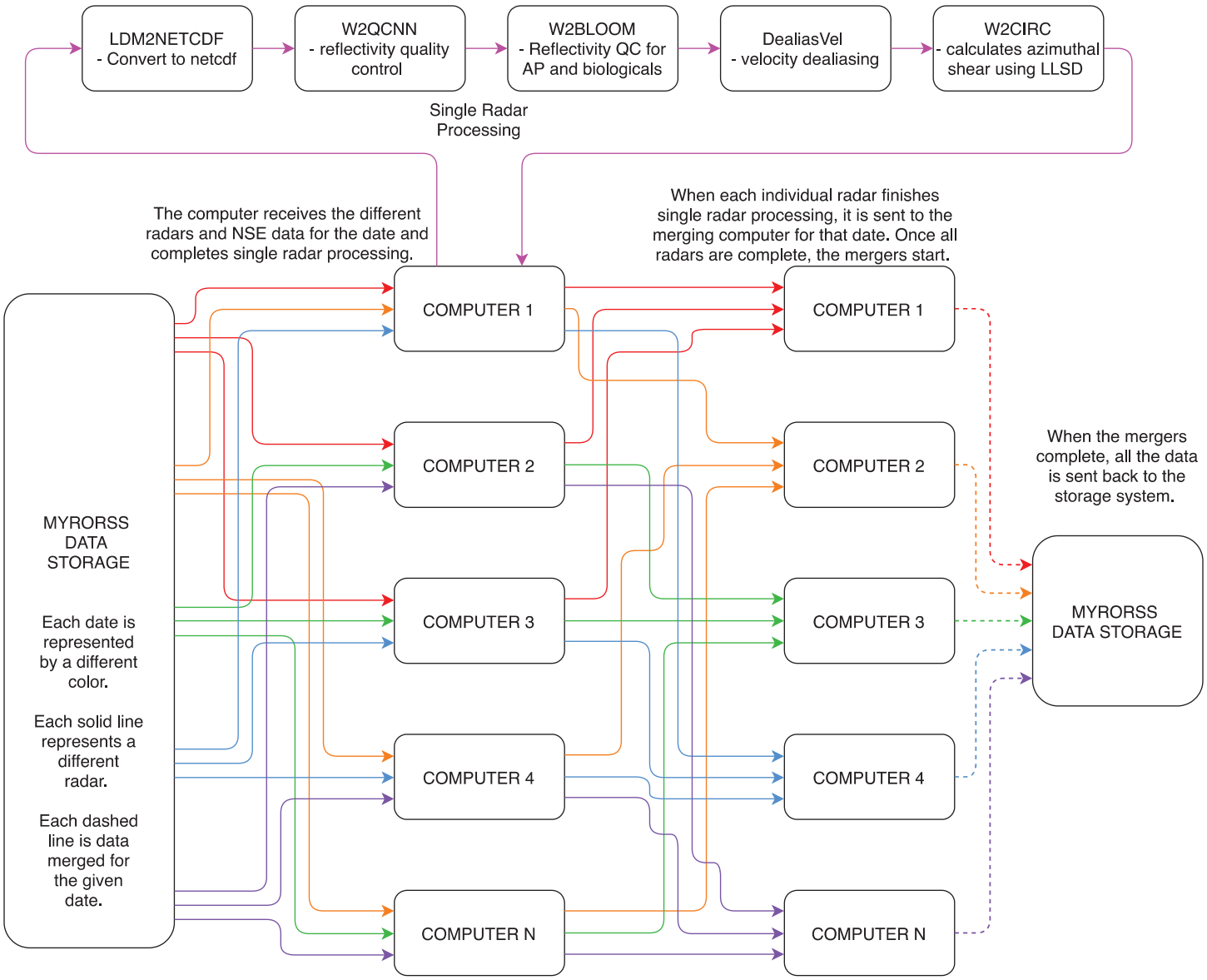

Fig. 1. Flowchart showing the complexities of processing such a large dataset and how it flows on a distributed computing system. Each color is representative of a different date to allow multiple dates and radar to be processed at once, each solid line is a different radar, and each dashed line is the final merged radar data. The single-radar processing flow is shown at the top of the figure and is completed for each radar. Single-radar data are stored as binary radial data, and NSE data are preprocessed into netCDF formatted latitude–longitude grids. Final data are in netCDF formatted latitude–longitude grids for each level of the merger and the two flattened azimuthal shear products.

The reflectivity field was blended in 3D while the azimuthal shear layers were blended in 2D using the maximal values in the layer. The horizontal resolutions for the reflectivity data and azimuthal shear layers are shown in Table 1. The temporal resolution is approximately every 5 min as the merger is triggered when the software receives data that are at least 5 min removed from the previously computed volume. The 3D reflectivity volume is a product itself but was also the input for several other radar-derived products that are discussed within the "Products" section. The 3D reflectivity has a staggered vertical grid with 35 levels (Table 1)

Computational and hardware configuration. The large amount of data were processed using a distributed computing system. The processing completed at CIWRO/NSSL leveraged up to 17 processing machines, with a single machine serving as the data storage (Fig. 1). These processing machines are individual computers equipped with 32–128 GB of RAM, and in general a minimum of 50 GB of RAM was needed to complete the three-dimensional

Table 1. Horizontal resolution of the reflectivity products and the azimuthal shear products.

MYRORSS horizontal resolution		
	Horizontal resolution	**Grid points**
Reflectivity products	0.01° latitude × 0.01° longitude, approximately 1-km^2 resolution	3,500 × 7,000 grid points
Azimuthal shear products	0.005° latitude × 0.005° longitude, approximately 0.5-km^2 resolution	7,000 × 14,000 grid points
MYRORSS reflectivity vertical resolution		
Height above MSL	**Vertical spacing**	**Levels**
250 m–3 km	250 m	12
3.5–9 km	500 m	12
10–20 km	1,000 m	11

reflectivity mergers, though some intense, widespread severe weather days (e.g., 27 April 2011 outbreak) required over 90 GB of RAM. Hard disk input/output (I/O) was the most restrictive bottleneck for processing and generally limited the processing on each machine to about twenty simultaneous processes. For intense, widespread severe weather, I/O would slow merger processing to near or slower than real time (i.e., an hour of elapsed time in the data were equivalent to a real-time hour of processing); however, increased storm coverage did not lead to significant changes in single-radar processing time. Figure 1 shows a simplified example of the workflow for processing. For each date, all the data were staged on the MYRORSS storage server and from there that machine sent out all the single radar processing to other, available processing computers. If machines were too busy, the storage server would wait and continue sending data once machines were available, automatically. Once the single-radar processing was completed, the data were transferred to the machine selected to run the merger processing. The merging process began once all valid radars for the day arrived on the machine, automatically. Once the merger processing was finished, the merged data were transferred back to the MYRORSS storage server.

The processing was monitored by CIWRO/NSSL staff and student assistants. Several checks were written into controlling software for the single-radar and merger processing, which would halt processing of that specific single-radar or merger process if a potential processing failure was detected. Users could then review the potential error, implement a potential solution (or in extreme cases, completely delete corrupted data), and then restart the processing where it left off. This reduced both the amount of potential missing data in the resulting dataset[3] and the amount of time required for processing to occur. Each archived year of data took approximately 1–1.5 months to process for legacy resolution radar data and 1.5–2 months to process for superres resolution radar data. Each year processed is approximately 5 TB of data, most of it being the three-dimensional reflectivity field.

[3] Since WDSS-II software runs in a linear fashion, a corrupt file or invalid data could prematurely end processing of data. If no checks were implemented, the data would be sent only partially complete and the resulting merger would be incomplete as well.

Additional quality control and known issues. While the reflectivity quality control software used in MYRORSS processing has been developed over many years and published (Lakshmanan et al. 2007b, 2010; Tang et al. 2011), there still arise situations where data errors were passed on by the software as valid reflectivity echoes. A common example of nonmeteorological reflectivity data still passing through the quality control software was the result of superrefraction of coastal radar signals when strong inversions were present, leading to radar beam ducting over the water surface (Doviak and Zrnić 2006). This caused scattering on coastlines far from the radar due to buildings and other human infrastructure. Since the assumption within the quality control software was that the beam would be at altitudes far above the surface at those distances from the radars, the software would interpret the high

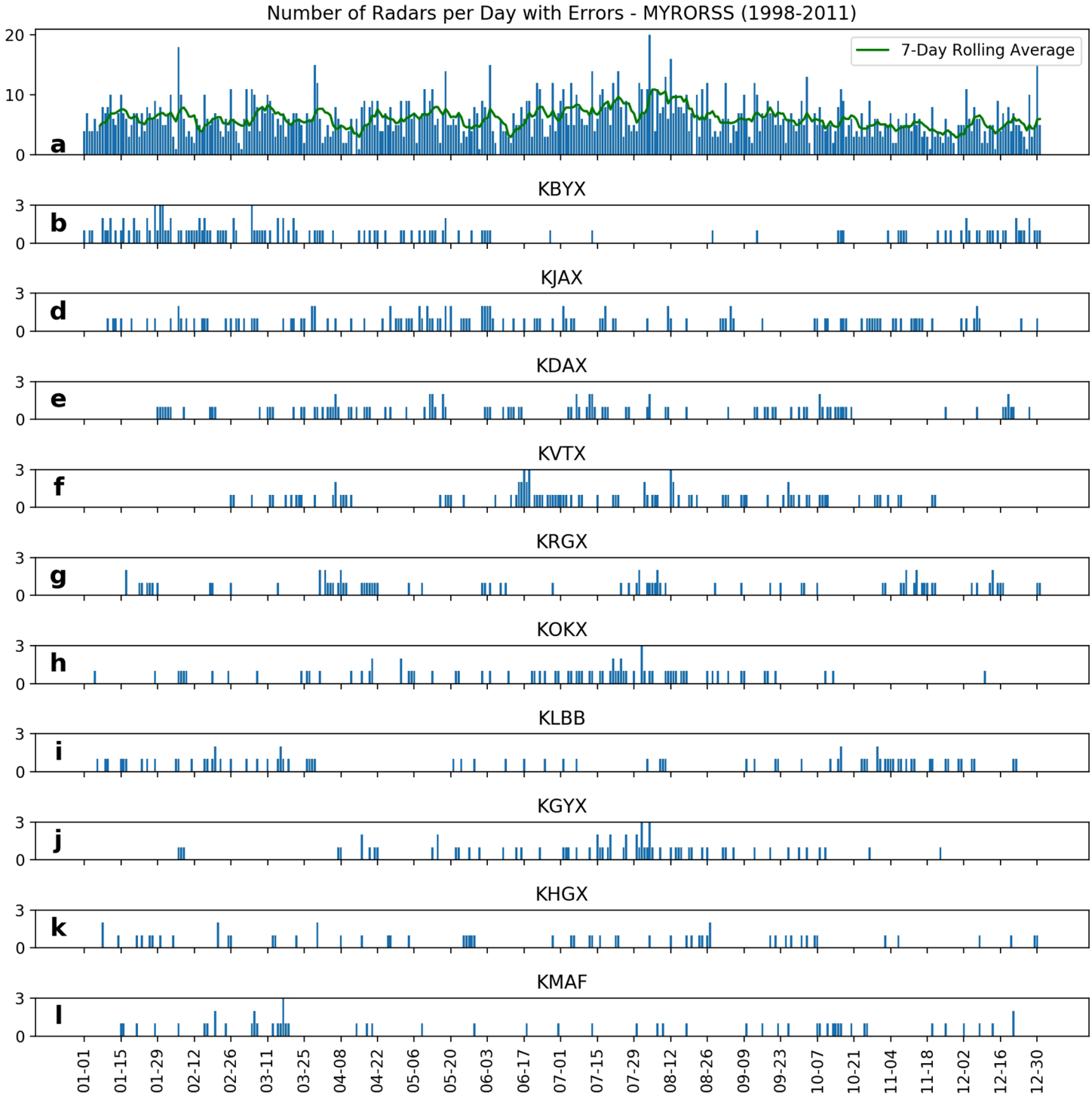

Fig. 2. (a) Number of radars per day with at least one error over the 14-yr dataset. (b)–(l) Top 10 radars (with KBYX being the highest) with at least one error or more.

reflectivity values from the ground clutter as valid weather signals. Another common failure was due to problems at the radar site and the encoding of the data. Frequently, individual elevation scans or even whole volumes, were nearly filled with very high reflectivity values (e.g., 90 dB*Z*), even for clear air. Another similar, but less frequent, issue was that the radar reflectivity would be offset by a large deviation (e.g., +50 dB*Z*), even for valid weather echoes. The number of radars per day with any type of error noted by the manual quality control is shown in Fig. 2 over the 14-yr dataset. Figures 2b–l show the top 10 radars with errors from the entire dataset over the 14-yr period. KBYX, located in Key West, Florida, is the radar with the most errors which mostly occur over the cool season. This radar, along with KJAX, KOKX,

KGYX, KHGX, and potentially also KVTX, had most of their errors due to the radar beam ducting over the water surface. The other radar errors were mostly due to terrain and electronic interference from chaff releases.

Since very high reflectivity values were generally the result of many of the data errors, each day of data could (somewhat) easily be manually inspected by a team of research assistants. This inspection was completed by viewing the daily accumulations of the MESH (Witt et al. 1998; Lakshmanan et al. 2007a; Smith et al. 2016) product, since large reflectivity at high altitudes would result in large MESH values. For MESH product patterns and values that looked to be in error, the source radar causing the probable invalid reflectivity was reviewed and if an error was found, the volume containing the error was removed and the date was reprocessed. If any false detections occurred while valid detections of weather were present (e.g., in another sector of the elevation scan), the corrupted data could not be removed without removing correct data and so they were not removed.

Ideally, the single-radar data would be remapped to the larger latitude–longitude domain by volume and stored. That would enable the capability to remove that data and rerun the merger process without having to reprocess the single-radar data. However, storage capacity limitations did not allow for this to occur, so even if only a single elevation scan was found to cause an error as described, the entire processing chain for all radars for the entire day would need to be rerun. In addition, if any single-radar processing changed, single-radar processing would still need to be completely rerun. Unfortunately, if this occurred, due to algorithm updates affecting the data, processing of the entire dataset had to be restarted several times since not all potential errors can be captured on testing datasets.

Since there was no additional Doppler velocity quality control beyond dealiasing of the data, azimuthal shear is highly susceptible to problems in the base data caused by radar site data corruptions and dealiasing errors. Further, no streamlined solution has been found for removing poor or invalid velocity data while retaining the uncorrupted reflectivity data. This is because radar data volume in the binary Level II format contains both reflectivity and velocity data. For MYRORSS processing in general, if the reflectivity was invalid, the removal of velocity data as well would not negatively impact the resulting azimuthal shear product (i.e., invalid reflectivity data always means invalid velocity data). However, the opposite was not true. Thus, the poor velocity data elevations would have to be individually targeted for removal and the workload required was infeasible for such a large dataset.

Corrupted data examples, shown in Fig. 3, exist even after the automated quality control algorithms. These examples include rings around the radar seemingly due to the corruption at the radar site with data collection (Fig. 3a), traffic on interstate highways and wind farms from strong temperature inversions near the radar (Fig. 3b), dealiasing failures appearing in the azimuthal shear product (Fig. 3c) and radar beam ducting along coasts (Fig. 3d). Even with noisy and incorrect data, users can still do postprocessing to "clean" the data a bit more. For example, an additional filter was applied to the MESH data in the MESH climatology (discussed in depth later) during postprocessing. This additional filter, a multiple hypothesis tracking (MHT) algorithm, was added to the accumulator algorithm within WDSS-II (Lakshmanan et al. 2013a) and aids in the removal of noise and erroneous data. The MHT algorithm required clusters to be of a certain size and remain for certain number of timeframes or else the data within those clusters were filtered out of the resulting product. If a cluster reached the size thresholds, then it must also meet the temporal threshold. This helped remove errors that only appear for one radar scan and immediately disappear in the next scan, remove clutter that has no movement, and filter lower, inconsequential MESH values from the final products.

The final remaining, potential complication of the MYRORSS database was the varying temporal resolution that was near the 5-min target interval. The merger process has an inherent

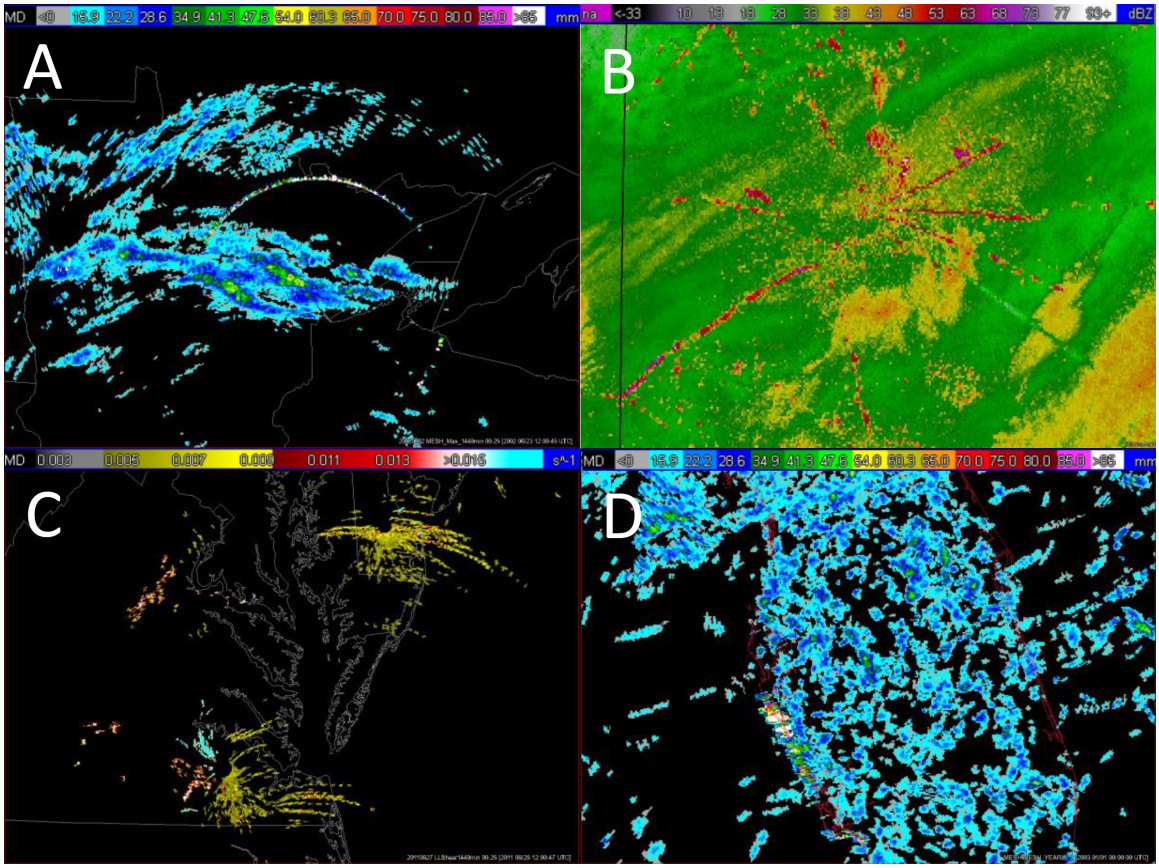

Fig. 3. Quality control issues: (a) ring shown around KDLH in MESH 24-h accumulation for 1200 UTC 22 Jun 2002–1200 UTC 23 Jun 2002, (b) interstate highways and windfarms in a monthly accumulation for February 2011 of reflectivity at lowest altitude centered over KAMA (from Smith et al. 2017), (c) a daily accumulation of positive low-level azimuthal shear in the Mid-Atlantic region showing where velocity dealiasing failed for 1200 UTC 27 Aug 2011–1200 UTC 28 Aug 2011, and (d) beam ducting appearing in the MESH product along the western coast of Florida for the 2002 accumulation.

0–2-s time drift each time a new data interval is processed. Thus, all time steps are at least 5 min, though rarely exactly 5 min.

It should be noted that only horizontally polarized reflectivity data were used for the three-dimensional merger and the database does not include the dual polarimetric era products, which will involve additional preprocessing of fields. New products, merger settings and resolutions have been tested for future processing of polarimetric data. Additional quality control will have to be implemented for polarimetric data, primarily for Z_{DR} calibration concerns.

Products

For the CONUS, 17 different products were created and saved within the MYRORSS dataset: 3D base reflectivity (Figs. 4a,b), composite reflectivity (Fig. 4c), reflectivity at the lowest altitude (RALA; Fig. 4d), echo tops at 18 dB*Z* (Fig. 5a), echo tops at 40 dB*Z* (Fig. 5b), echo tops at 50 dB*Z* (Fig. 5c), height of 18-dB*Z* echo tops above the 0°C isotherm (Fig. 5d), height of 40-dB*Z* echo tops above the 0°C isotherm (Fig. 5e), height of 50-dB*Z* echo tops above the 0°C isotherm (Fig. 5f), reflectivity at isotherm 0°C (Fig. 6a), reflectivity at isotherm −10°C (Fig. 6b), reflectivity at isotherm −20°C (Fig. 6c), MESH (Fig. 6d), vertically integrated liquid (VIL; Fig. 6e), severe hail index (SHI; Fig. 6f), 0–3 km AGL azimuthal shear (Fig. 7a), and 3–6 km AGL azimuthal shear (Fig. 7b). Information about each product is summarized in Table 2. The products saved by the reanalysis were determined by usability and popularity, allowing inexperienced users to be able to work with data without additional 3D cube algorithm processing.

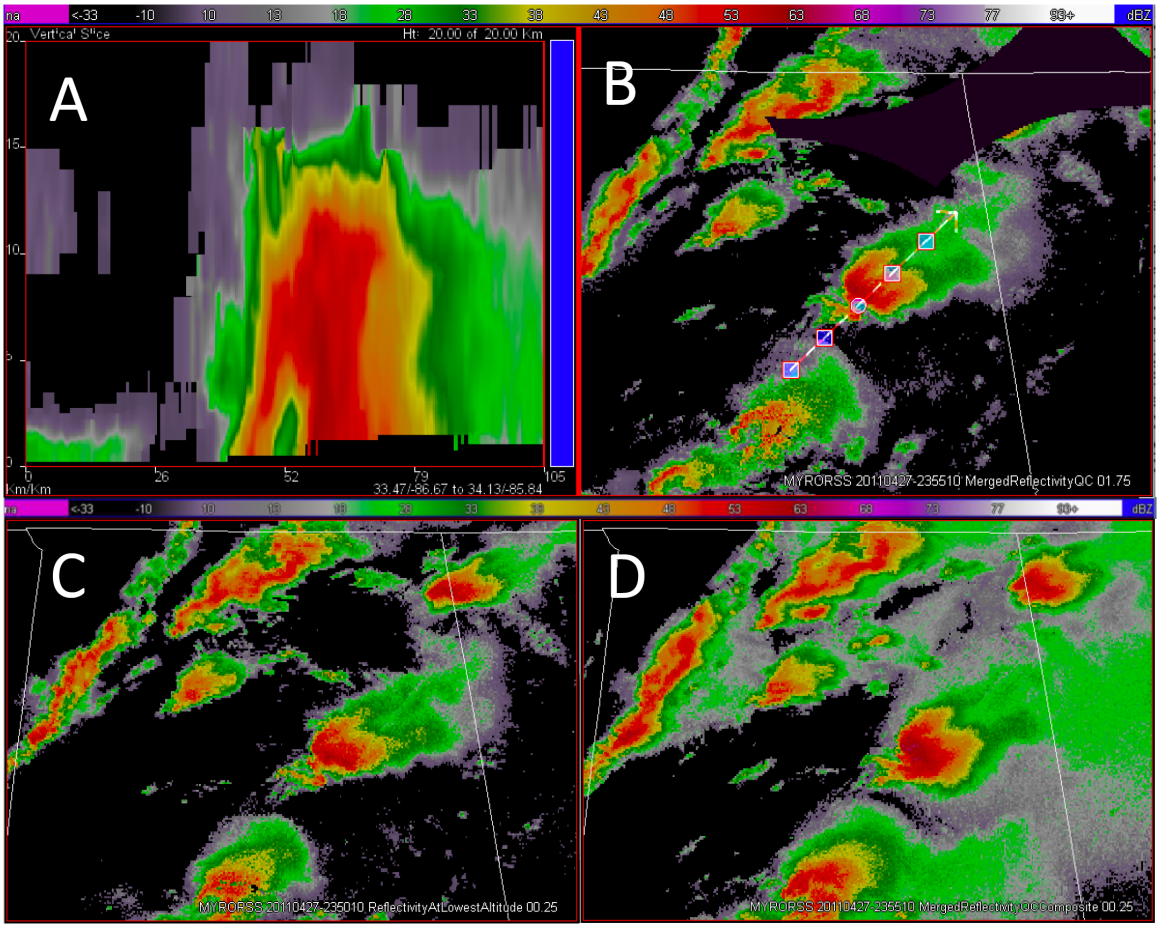

Fig. 4. (a) Vertical cross section of reflectivity with (b) composite reflectivity at 1.25 km and cross-section location, (c) reflectivity at lowest altitude, and (d) composite reflectivity at 2355 UTC 27 Apr 2011.

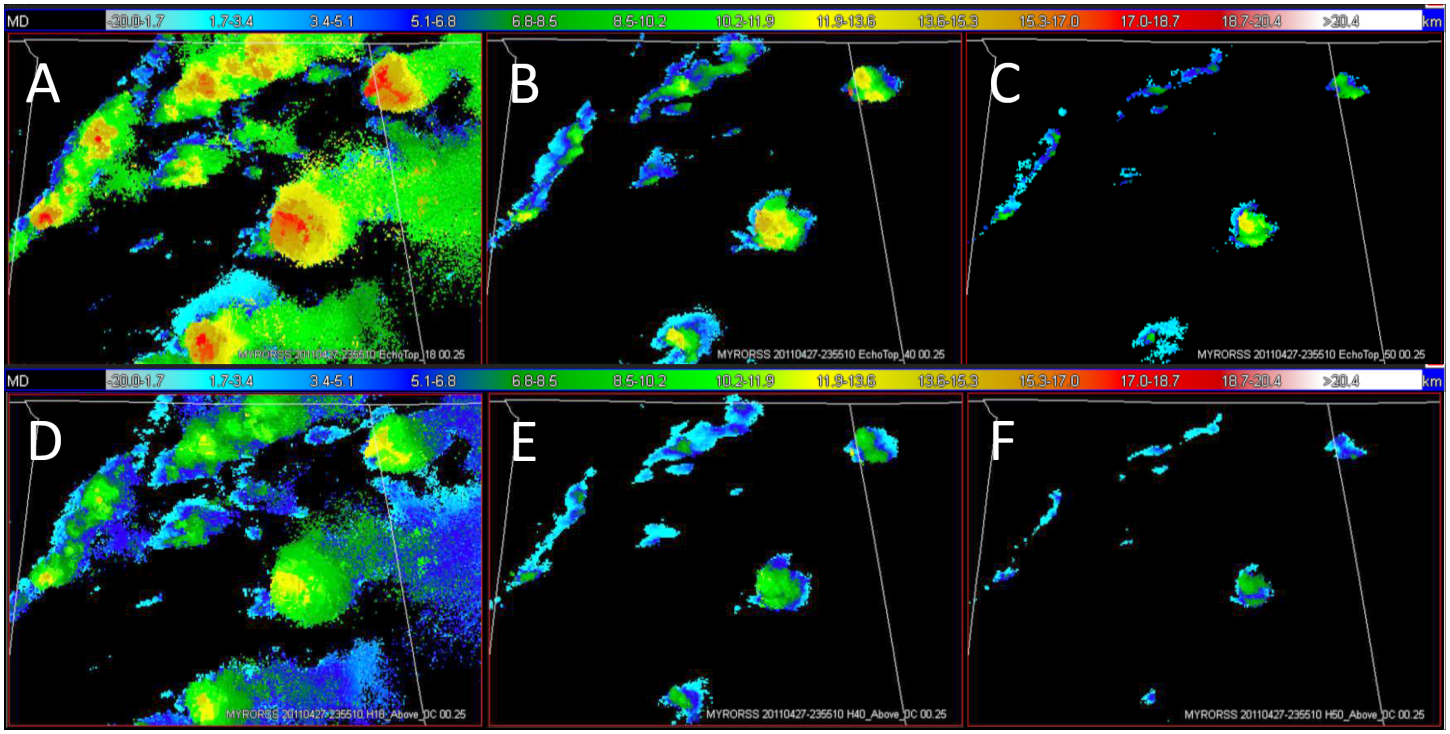

Fig. 5. Echo tops at (a) 18, (b) 40, and (c) 50 dBZ. Height of (d) 18-, (e) 40-, and (f) 50-dBZ echo top above the 0°C isotherm at 2355 UTC 27 Apr 2011.

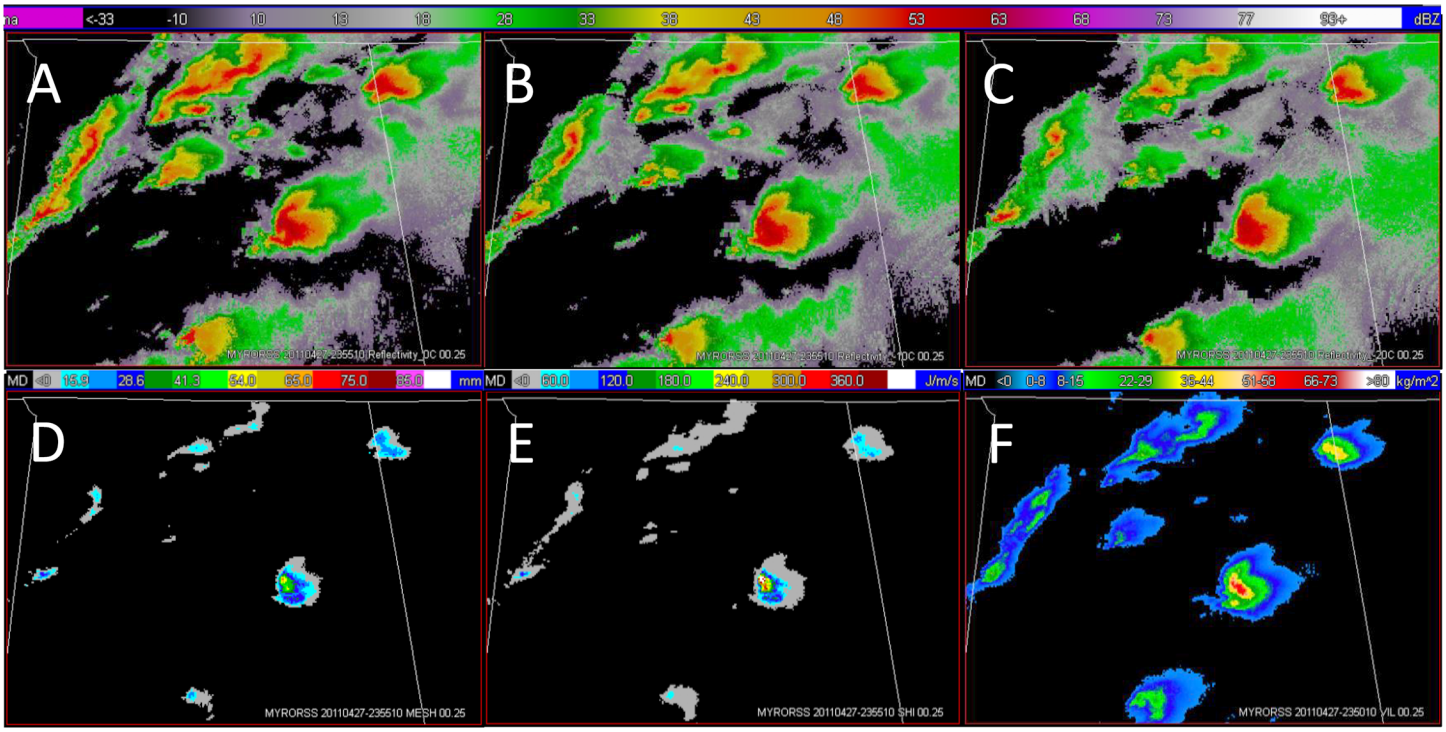

Fig. 6. Selection of reflectivity-based products (bottom row) produced for the MYRORSS dataset. Reflectivity at isotherm (a) 0°, (b) –10°, and (c) –20°C. Radar derived products (d) MESH, (e) SHI, and (f) VIL at 2355 UTC 27 Apr 2011.

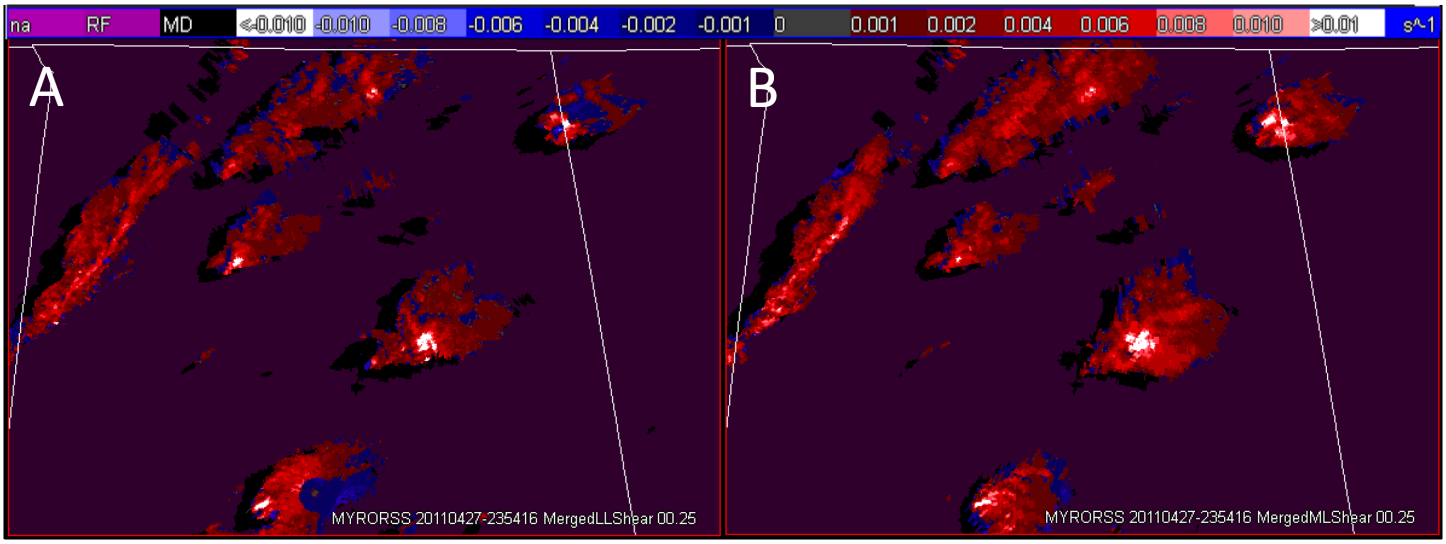

Fig. 7. The two Doppler-derived velocity products produced for the MYRORSS dataset. (a) Low-level and (b) midlevel azimuthal shear at 2354 UTC 27 Apr 2011.

Summary of research using MYRORSS

Several projects have been underway as the MYRORSS data were being processed and quality controlled. The temporal span of the data lends itself toward developing climatologies while the large size of the dataset makes it sufficient for machine learning, especially deep learning. MYRORSS MESH data have been explored to create new hail climatologies for the United States. So far general investigations of the number of days of hail per year, seasonality of hail occurrence (Layne et al. 2014; Rosseau et al. 2017), and preferred day of the week and time of day have been conducted (Williams et al. 2018). Hourly swaths of multiple products combined with near-storm environment data are being explored as the input to machine learning methods to hopefully develop better hail sizing algorithms and to develop a better hail

Table 2. The MYRORSS product names along with the usefulness of each product, the figure of the example, and references to the algorithm.

MYRORSS products			
Product name (unit)	**About/uses**	**Image**	**References**
3D base reflectivity (dB*Z*)	Gives complete overview of storm Used to create many of the other products within MYRORSS	Figs. 4a,b	Smith et al. (2016)
Composite reflectivity (dB*Z*)	Maximum value of reflectivity in the vertical column above each grid point Used to view full horizontal extent of storms at all altitudes that a specific tilt may not encompass	Fig. 4d	Tait et al. (2015)
Reflectivity at lowest altitude (dB*Z*)	Reflectivity value closest to Earth's surface Useful to indicate intensity of precipitation near the surface	Fig. 4c	Smith et al. (2016)
Echo tops at 18, 40, and 50 dB*Z* (km)	Highest altitude of the specified reflectivity value Useful for identifying rapidly intensifying convection and determining storm severity	Figs. 5a–c	Lakshmanan et al. (2013b), Smith et al. (2016)
18-, 40-, and 50-dB*Z* echo top height above 0°C isotherm (km)	Identification of strong updrafts and potential for severe hail	Figs. 5d–f	Cavanaugh and Schultz (2012)
Reflectivity at 0°, –10°, and –20°C (dB*Z*)	Reflectivity at isotherms are based on environmental temperature from RUC analyses Useful for detection of hail growth and identifying which storms will likely produce lightning	Figs. 6a–c	Smith et al. (2016)
Maximum expected size of hail (MESH; mm)	Shows full spatial extent and hail size distribution of a thunderstorm	Fig. 6d	Witt et al. (1998), Lakshmanan et al. (2006)
Severe hail index (SHI; J m^{-1} s^{-1})	Used as input to MESH	Fig. 6e	Witt et al. (1998), Lakshmanan et al. (2006)
Vertically integrated liquid (VIL; kg m^{-2})	Measure of the liquid water content within a cloud High values have been frequently associated with severe weather	Fig. 6f	Greene and Clark (1972), Smith et al. (2016)
Low- and midlevel azimuthal shear (s^{-1})	Indicative of rotation within a storm including mesocyclones and tornadic vortex signatures depending on level of viewing Gust fronts near radar can overwhelm signal leading to noisy/erroneous data Not calculated within 5 km of radar or when velocity data are range folded or missing	Figs. 7a,b	Smith and Elmore (2004), Mahalik et al. (2019)

climatology beyond simple classification thresholds (e.g., severe versus nonsevere; Meadows et al. 2021). One outcome from these preliminary investigations into creating the climatology is that even with extensive quality control, issues can still be seen in the maximal MESH (Fig. 8a), such as a radar ring in northeastern Minnesota and high maximal MESH values in central California where radar beams interact with topography. Other quality control issues are also apparent using the MESH counts (Fig. 8b) with high counts in central California again and along the coasts in Florida due to beam ducting (shown closer in Fig. 3d).

A rotating storms climatology has been examined as well. Using the azimuthal shear products from MYRORSS, the occurrence of storm rotation across the CONUS was examined first by Williams et al. (2014), but due to an error with the LLSD algorithm, the analysis had to be reprocessed. Smith and Ortega (2017) compared the azimuthal shear from the original algorithm to the corrected algorithm, while LaRoche et al. (2018) continued with the work and investigated different methods on how to filter out noisy data due to gust fronts while still maintaining the rotation tracks. MHT was again leveraged to filter the azimuthal shear product when creating rotation tracks. The aggressive MHT settings (Fig. 9c) maintained the strongest rotation tracks but filtered out the weaker tracks that had the potential to be tornadoes while the conservative MHT settings (Fig. 9b) left too much noise along fronts especially when a location was close to a radar site. Additional work is being completed still to determine the best settings and other quality control methods.

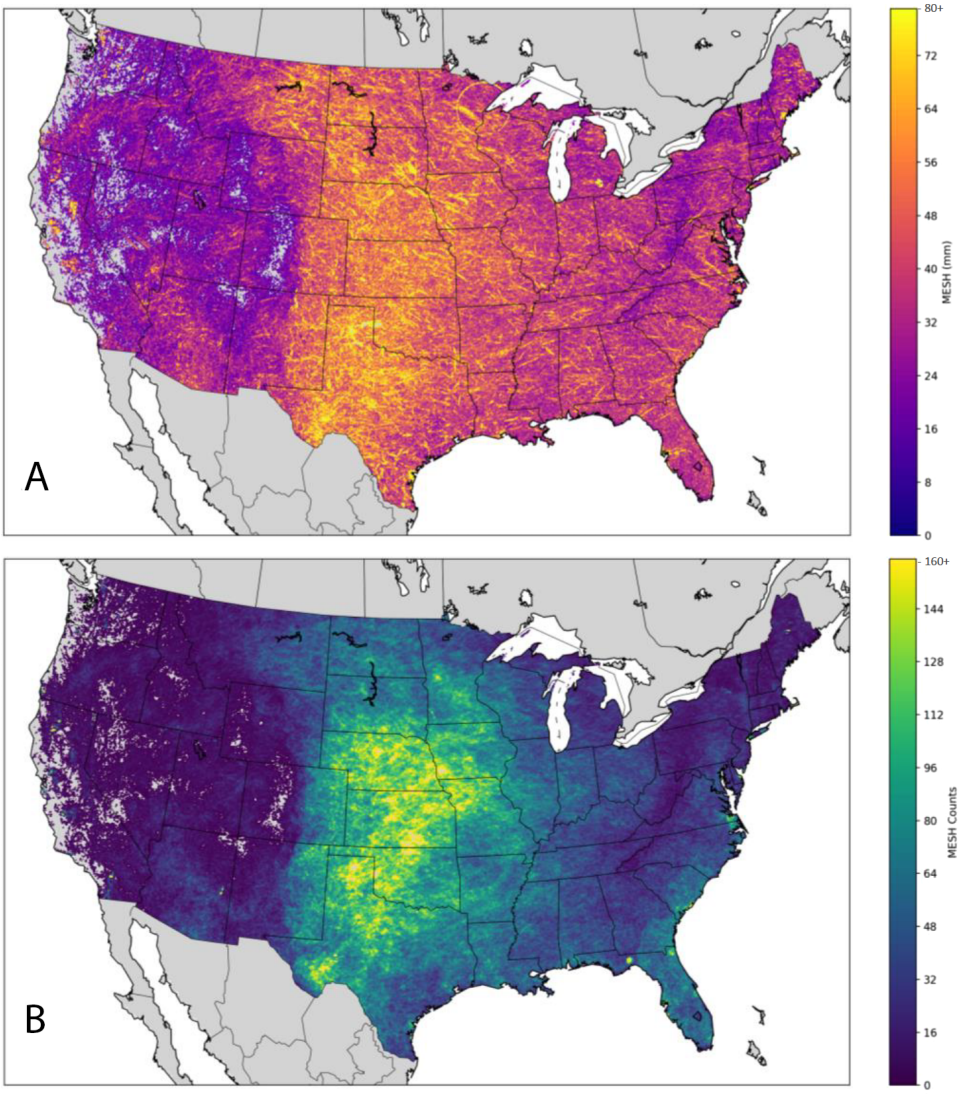

Fig. 8. A simple example of a climatological application of MYRORSS data with (a) maximal MESH and (b) counts of any sized MESH for the entire dataset produced thus far (1998–2011).

Smith et al. (2017) completed a reflectivity climatology using the reflectivity products including merged reflectivity, composite reflectivity, isothermal reflectivities as 0°, –10°, and –20°C, as well as RALA. This showed the seasonal and monthly climatologies at the –10°C isotherm and showed contamination from wind farms, interstate highways, and other quality control issues. Kingfield et al. (2017) examined the 50-dBZ echo tops for 2000–11. Their work showed the maximum height over the 12-yr period, the number of occurrences per year of certain heights and greater, and the seasonal and hourly distributions. The study also included the distributions of NSE analyses for the distribution of 50-dBZ echo top heights for Nebraska and Florida. The conclusions showed that the central plains had the highest continuous coverage of 50-dBZ echo tops with summer being the most active in extent and intensity. The deepest cells in this region occurred between 1800 and 0300 UTC. Additionally, hourly swaths of the echo tops are being leveraged to develop a general storm climatology for the United States (Ferguson et al. 2021).

An important application of the MYRORSS dataset is for use in numerical weather prediction (NWP) model verification and in the use of Data Assimilation for NWP, specifically convective allowing models (CAMs). The gridded nature and consistent quality control of the dataset allows for a pristine truth dataset that can be used in CAM verification and validation. Previously, object-based verification methods used Stage IV QPE products as

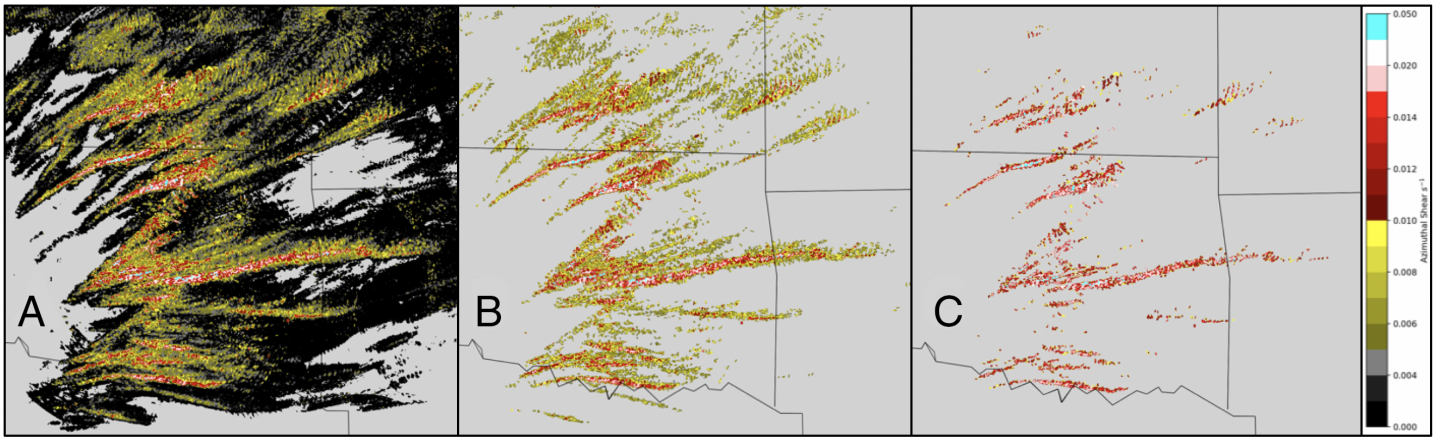

Fig. 9. An example of the preprocessing of data fields needed prior to any sort of application of the data. Here, (a) raw azimuthal shear data were filtered by (b) low and (c) high MHT settings for filtering azimuthal shear.

the truth against reflectivity and Weather Research and Forecasting (WRF) Model output (Ebert and McBride 2000; Baldwin et al. 2005; Davis et al. 2006). The quality of the dataset easily allows for object identification and matching between reflectivity datasets instead of reflectivity proxies. Using MYRORSS reflectivity products instead of Stage IV QPE data to represent convection allows for a more realistic verification between model reflectivity and observed reflectivity and impacts associated with reflectivity other than rainfall from the WSR-88D network (Skinner et al. 2018; Gallo et al. 2019; Potvin et al. 2019; Johnson et al. 2020). Another project being completed involves pairing NWS severe and tornado warnings with the MYRORSS data and *Storm Data* reports to create a machine learning model to predict the probability of an NWS warning verifying (Douglas et al. 2021).

MYRORSS is an ideal dataset to be used for machine learning applications due to the millions of data points available over a 14-yr period. Machine learning work has been utilized for prediction of damaging straight-line wind (≥50 kt or 25.7 m s^{-1}) using the data from MYRORSS for July 2001 through December 2011, excluding 2009 (Lagerquist et al. 2017), and for tornadoes for the next hour using convolutional neural networks (CNN; Lagerquist et al. 2020). For hail size prediction and classification, machine learning techniques, including fully connected neural networks, deep-learning, and gradient boosted decision trees, have been used to investigate the MYRORSS data combined with the Severe Hazards Analysis and Verification Experiments (SHAVE) hail reports (Williams and Ortega 2019), as well as hail reports from *Storm Data* (Escamilla et al. 2020). Using the reflectivity vertical profiles, as well as the derived radar products, such as azimuthal shear, MESH, and VIL, at the location of a report as inputs to the networks, hail size was predicted. These initial results have shown improvement of hail prediction compared to using solely MESH but have also shown that vertical profiles alone cannot predict hail size. While results had lower mean absolute errors than MESH (Fig. 10), the spread in predictions still existed. For example, an observed hail size of 75 mm had predictions using a gradient boosted decision tree ranging from 10 up to 75 mm, which was similar for MESH distributions of the same data. In addition to SHAVE reports, similar work has been completed with *Storm Data* that showed nearly identical results (Escamilla et al. 2020).

A derivative of the MYRORSS dataset includes storm objects (Clough et al. 2021). These objects are created for two different *k*-means watershed segmentation methods. The "lightning" object settings are from Meyer et al. (2017), while the more mesoscale-sized feature settings are from the ProbSevere Model (Cintineo et al. 2018). The number of storm objects from the ProbSevere segmentation settings for April 2011 was over 200,000. It is estimated that there are over 15 million objects in the entire dataset. These objects not only contain the reflectivity

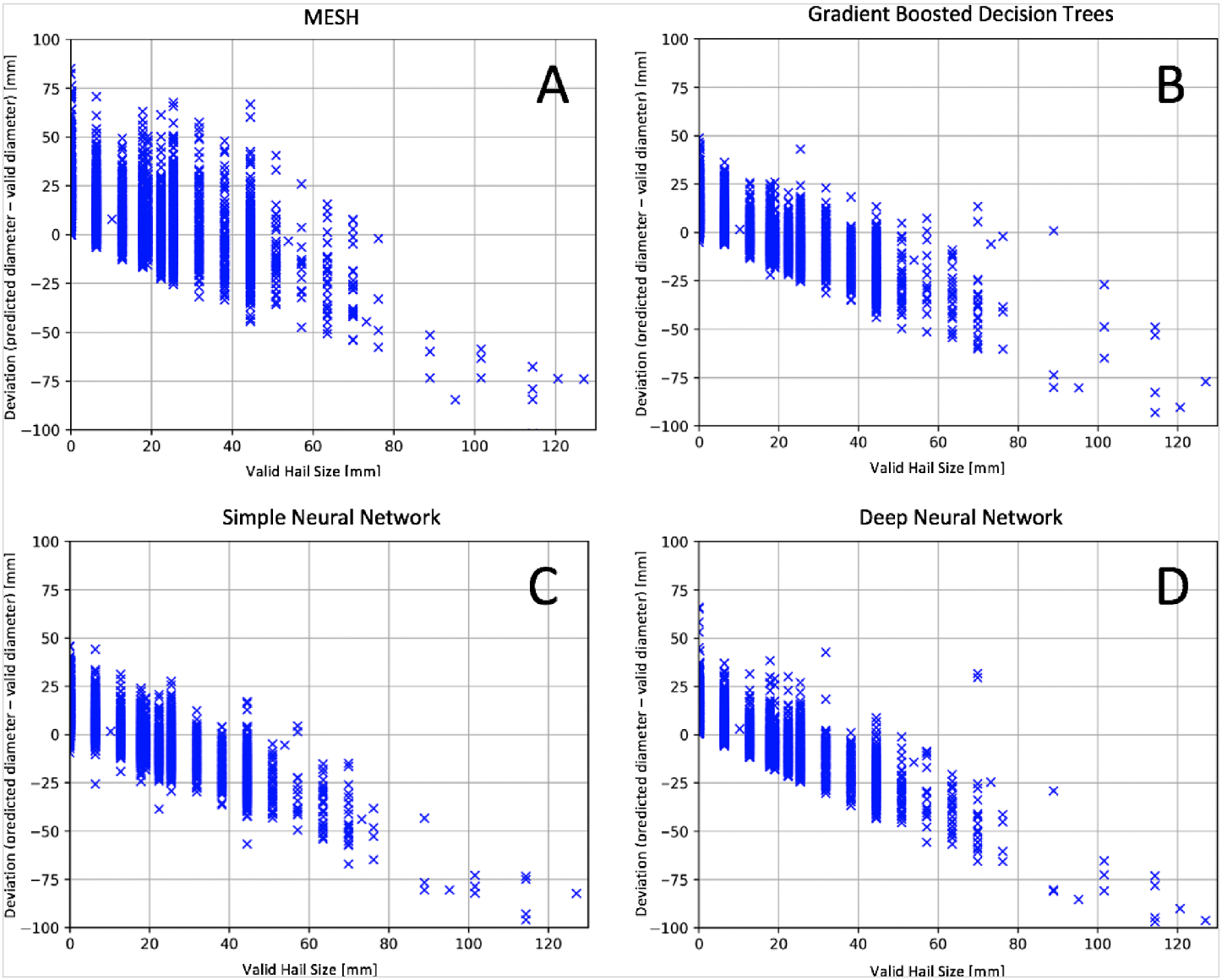

Fig. 10. Relative derivative of predicted values for hail size predictions using machine learning models. (a) MESH—mean absolute error (MAE): 14.50 mm, (b) gradient boosted decision trees—MAE: 9.17 mm, (c) simple neural network—MAE: 9.99 mm, and (d) deep neural network—MAE: 10.03 mm.

information, but also include more than 1,200 attributes from the MYRORSS MRMS and NSE fields. These objects are also paired with information about population, land use, and *Storm Data*. The storm object attributes are saved in comma-separated values (CSV) files to create a more user-friendly version of the MYRORSS dataset. Current work involving the storm objects include creating machine learning models to predict the probability of convective hazard given the attribute information.

The nearly 14 years of processed MYRORSS data have been used for many applications and has proven to be useful. Currently, the workflow is under development for future processing of dual-pol radar data. With the additional polarimetric variables available, different methods for merging these products are being investigated, as well as any other additional products that could be included moving forward. Because of the large amount of data associated with dual-pol radar, additional computing resources will be utilized including the University of Oklahoma's OU Supercomputing Center for Education and Research (OSCER) to increase processing abilities. This would allow for multiple years to be processed concurrently in house on the distributed system as well as on the supercomputer. The MYRORSS dataset is now publicly available at https://doi.org/10.15763/DBS.CIMMS.MYRORSS.

Acknowledgments. Funding was provided by NOAA/Office of Oceanic and Atmospheric Research under NOAA–University of Oklahoma Cooperative Agreement NA16OAR4320115, U.S. Department of Commerce. Some of the data analyses shown using MYRORSS were performed at the OU Supercomputing Center for Education and Research (OSCER) at the University of Oklahoma (OU).

Data availability statement. MYRORSS data and information are provided by OU/CIWRO and are available at https://doi.org/10.15763/DBS.CIMMS.MYRORSS. The WDSS-II software is available by contacting Kiel Ortega (kiel.ortega@noaa.gov).

References

Ansari, S., and Coauthors, 2018: Unlocking the potential of NEXRAD data through NOAA's big data partnership. *Bull. Amer. Meteor. Soc.*, **99**, 189–204, https://doi.org/10.1175/BAMS-D-16-0021.1.

Baldwin, M. E., J. S. Kain, and S. Lakshmivarahan, 2005: Development of an automated classification procedure for rainfall systems. *Mon. Wea. Rev.*, **133**, 844–862, https://doi.org/10.1175/MWR2892.1.

Benjamin, S. G., and Coauthors, 2004: An hourly assimilation–forecast cycle: The RUC. *Mon. Wea. Rev.*, **132**, 495–518, https://doi.org/10.1175/1520-0493(2004)132<0495:AHACTR>2.0.CO;2.

Cavanaugh, D. E., and J. A. Schultz, 2012: WSR-88D signatures associated with one inch hail in the Southern Plains. *Electron. J. Oper. Meteor.*, **13**, 1–14.

Cintineo, J. L., and Coauthors, 2018: The NOAA/CIMSS ProbSevere model: Incorporation of total lightning and validation. *Wea. Forecasting*, **33**, 331–345, https://doi.org/10.1175/WAF-D-17-0099.1.

Clough, K. N., S. S. Williams, and K. L. Ortega, 2021: Developing a Multi-Radar, Multi-Sensor storm database using the multi-year reanalysis of remotely sensed storms. *20th Annual Student Conf.,* Virtual, Amer. Meteor. Soc., 21, https://ams.confex.com/ams/101ANNUAL/meetingapp.cgi/Paper/385058.

Davis, C. A., B. G. Brown, and R. G. Bullock, 2006: Object-based verification of precipitation Forecasts. Part I: Methodology and application to mesoscale rain areas. *Mon. Wea. Rev.*, **134**, 1772–1784, https://doi.org/10.1175/MWR3145.1.

Douglas, Z. A., S. S. Williams, and K. L. Ortega, 2021: Developing verification probabilities for NWS warning polygons using MRMS. *20th Annual Student Conf.,* Virtual, Amer. Meteor. Soc., 132, https://ams.confex.com/ams/101ANNUAL/meetingapp.cgi/Paper/385031.

Doviak, R. J., and D. S. Zrnić, 2006: *Doppler Radar and Weather Observations.* Academic Press, 592 pp.

Ebert, E. E., and J. L. McBride, 2000: Verification of precipitation in weather systems: Determination of systematic errors. *J. Hydrol.*, **239**, 179–202, https://doi.org/10.1016/S0022-1694(00)00343-7.

Escamilla, J. E. A., S. S. Williams, and K. L. Ortega, 2020: MRMS-based hail sizing and classification using different large databases. *19th Conf. on Artificial Intelligence for Environmental Science*, Boston, MA, Amer. Meteor. Soc., 363192, https://ams.confex.com/ams/2020Annual/webprogram/Paper363192.html.

Ferguson, C. K., S. S. Williams, and K. L. Ortega, 2021: Developing a general storm climatology using 1-hourly swaths of MRMS echo tops. *20th Annual Student Conf.,* Virtual, Amer. Meteor. Soc., 17, https://ams.confex.com/ams/101ANNUAL/meetingapp.cgi/Paper/385028.

Gallo, B. T., and Coauthors, 2019: Initial development and testing of a convection-allowing model scorecard. *Bull. Amer. Meteor. Soc.*, **100**, ES367–ES384, https://doi.org/10.1175/BAMS-D-18-0218.1.

Greene, D. R., and R. A. Clark, 1972: Vertically integrated liquid water—A new analysis tool. *Mon. Wea. Rev.*, **100**, 548–552, https://doi.org/10.1175/1520-0493(1972)100<0548:VILWNA>2.3.CO;2.

Jing, Z., and G. Wiener, 1993: Two-dimensional dealiasing of Doppler velocities. *J. Atmos. Oceanic Technol.*, **10**, 798–808, https://doi.org/10.1175/1520-0426(1993)010<0798:TDDODV>2.0.CO;2.

Johnson, A., X. Wang, Y. Wang, A. Reinhart, A. J. Clark, and I. L. Jirak, 2020: Neighborhood- and object-based probabilistic verification of the OU MAP ensemble forecasts during 2017 and 2018 hazardous weather testbeds. *Wea. Forecasting*, **35**, 169–191, https://doi.org/10.1175/WAF-D-19-0060.1.

Kingfield, D. M., K. L. Ortega, and T. C. Meyer, 2017: A terrestrial multi-radar echo top climatology of the continental United States derived from MYRORSS: 2000–2012. *18th Conf. on Aviation, Range, and Aerospace Meteorology*, Seattle, WA, Amer. Meteor. Soc., 14.4, https://ams.confex.com/ams/97Annual/webprogram/Paper302944.html.

Lagerquist, R., A. McGovern, and T. Smith, 2017: Machine learning for real-time prediction of damaging straight-line convective wind. *Wea. Forecasting*, **32**, 2175–2193, https://doi.org/10.1175/WAF-D-17-0038.1.

——, ——, C. R. Homeyer, D. J. Gange II, and T. Smith, 2020: Deep learning on three-dimensional multiscale data for next-hour tornado prediction. *Mon. Wea. Rev.*, **148**, 2837–2861, https://doi.org/10.1175/MWR-D-19-0372.1.

Lakshmanan, V., T. M. Smith, K. Hondl, G. J. Stumpf, and A. Witt, 2006: A real-time, three-dimensional, rapidly updating, heterogeneous radar merger technique for reflectivity, velocity, and derived products. *Wea. Forecasting*, **21**, 802–823, https://doi.org/10.1175/WAF942.1.

——, ——, G. J. Stumpf, and K. D. Hondl, 2007a: The Warning Decision Support System–Integrated Information. *Wea. Forecasting*, **22**, 596–612, https://doi.org/10.1175/WAF1009.1.

——, A. Fritz, T. M. Smith, K. Hondl, and G. J. Stumpf, 2007b: An automated technique to quality control radar reflectivity data. *J. Appl. Meteor.*, **46**, 288–305, https://doi.org/10.1175/JAM2460.1.

——, J. Zhang, and K. Howard, 2010: A technique to censor biological echoes in radar reflectivity data. *J. Appl. Meteor. Climatol.*, **49**, 453–462, https://doi.org/10.1175/2009JAMC2255.1.

——, M. Miller, and T. Smith, 2013a: Quality control of accumulated fields by applying spatial and temporal constraints. *J. Atmos. Oceanic Technol.*, **30**, 745–758, https://doi.org/10.1175/JTECH-D-12-00128.1.

——, T. M. Smith, C. K. Potvin, and D. Preignitz, 2013b: An improved method for estimating radar echo-top height. *Wea. Forecasting*, **28**, 481–488, https://doi.org/10.1175/WAF-D-12-00084.1.

LaRoche, K., S. S. Williams, K. L. Ortega, A. E. Reinhart, M. C. Mahalik, B. R. Smith, and T. M. Smith, 2018: Using the MYRORSS database to create a rotating storms climatology. *29th Conf. on Severe Local Storms*, Stowe, VT, Amer. Meteor. Soc., 4, https://ams.confex.com/ams/29SLS/webprogram/Paper348649.html.

Layne, G. W., K. L. Ortega, H. E. Brooks, and T. M. Smith, 2014: A radar-based hail climatology for the CONUS (2000–2011). *27th Conf. on Severe Local Storms*, Madison, WI, Amer. Meteor. Soc., 144, https://ams.confex.com/ams/27SLS/webprogram/Paper255327.html.

Mahalik, M., B. Smith, K. Elmore, D. Kingfield, K. Ortega, and T. Smith, 2019: Estimates of gradients in radar moments using a linear least-squares derivative technique. *Wea. Forecasting*, **34**, 415–434, https://doi.org/10.1175/WAF-D-18-0095.1.

Meadows, D. K., K. L. Ortega, and S. S. Williams, 2021: Developing a hail climatology using MRMS swaths and machine learning. *20th Annual Student Conf.,* Virtual, Amer. Meteor. Soc., 18, https://ams.confex.com/ams/101ANNUAL/meetingapp.cgi/Paper/385030.

Meyer, T. C., K. M. Calhoun, D. M. Kingfield, and C. Karstens, 2017: Using random forest to generate probability of cloud-to-ground lightning probabilities. *38th Conf. on Radar Meteorology*, Chicago, IL, 5B.6, https://ams.confex.com/ams/38RADAR/meetingapp.cgi/Paper/320597.

NOAA/NWS/ROC, 1991: NOAA Next Generation Radar (NEXRAD) Level 2 Base Data. NOAA National Centers for Environmental Information, accessed 7 December 2020, https://doi.org/10.7289/V5W9574V.

Potvin, C. K., and Coauthors, 2019: Systematic comparison of convection-allowing models during the 2017 NOAA HWT spring forecasting experiment. *Wea. Forecasting*, **34**, 1395–1416, https://doi.org/10.1175/WAF-D-19-0056.1.

Rew, R. K., G. P. Davis, S. Emmerson, and H. Davies, 2015: NetCDF user's guide for C: An interface for data access. Unidata, UCAR, www.unidata.ucar.edu/software/netcdf/guide_toc.html.

Rosseau, D., K. L. Ortega, A. E. Reinhart, and H. Obermeier, 2017: A multi-radar, multi-sensor hail climatology for the CONUS: 2000-2011. *Special Symp. on Severe Local Storms: Observation Needs to Advance Research, Prediction, and Communication*, Seattle, WA, Amer. Meteor. Soc., 930, https://ams.confex.com/ams/97Annual/webprogram/Paper312563.html.

Skinner, P. S., and Coauthors, 2018: Object-based verification of a prototype warn-on-forecast system. *Wea. Forecasting*, **33**, 1225–1250, https://doi.org/10.1175/WAF-D-18-0020.1.

Smith, B. R., and K. L. Ortega, 2017: An updated radar-based storm rotation climatology for the CONUS. *38th Conf. on Radar Meteorology*, Chicago, IL, Amer. Meteor. Soc., 178, https://ams.confex.com/ams/38RADAR/webprogram/Paper320979.html.

——, ——, A. E. Reinhart, M. C. Mahalik, and T. M. Smith, 2017: A reflectivity climatology study of the contiguous United States using the Multi-Year Reanalysis of Remotely Sensed Storms (MYRORSS). *28th Conf. on Weather Forecasting/24th Conf. on Numerical Weather Prediction*, Seattle, WA, Amer. Meteor. Soc., 99, https://ams.confex.com/ams/97Annual/webprogram/Paper313436.html.

Smith, T. M., and K. L. Elmore, 2004: The use of radial velocity derivatives to diagnose rotation and divergence. *11th Conf. on Aviation, Range, and Aerospace*, Hyannis, MA, Amer. Meteor. Soc., P5.6, https://ams.confex.com/ams/pdfpapers/81827.pdf.

——, and Coauthors, 2016: Multi-Radar Multi-Sensor (MRMS) severe weather and aviation products. *Bull. Amer. Meteor. Soc.*, **97**, 1617–1630, https://doi.org/10.1175/BAMS-D-14-00173.1.

Tait, C., V. Passetti, and S. Abelman, 2015: Federal Aviation Administration Multi-Radar Multi-Sensor System research to operations accomplishments. *17th Conf. on Aviation, Range, and Aerospace Meteorology*, Phoenix, AZ, Amer. Meteor. Soc., 312, https://ams.confex.com/ams/95Annual/webprogram/Paper258567.html.

Tang, L., J. Zhang, Y. Wang, and K. Howard, 2011: Identification of biological and anomalous propagation echoes in weather radar observations—An imaging processing approach. *35th Conf. on Radar Meteorology*, Pittsburgh, PA, Amer. Meteor. Soc., 123, https://ams.confex.com/ams/35Radar/webprogram/Paper191296.html.

Torres, S. M., and C. D. Curtis, 2007: Initial implementation of super-resolution data on the NEXRAD network. *23rd Conf. on IIPS*, San Antonio, TX. Amer. Meteor. Soc., 5B.10, https://ams.confex.com/ams/87ANNUAL/techprogram/paper_116240.htm.

Williams, S. S., and K. L. Ortega, 2019: Developing a machine learning–based hail climatology using the SHAVE and MYRORSS databases. *Fifth Symp. on High Performance Computing for Weather, Water, and Climate*, Phoenix, AZ, Amer. Meteor. Soc., 327, https://ams.confex.com/ams/2019Annual/webprogram/Paper351515.html.

——, ——, D. M. Kingfield, and T. M. Smith, 2014: A radar-based storm rotation climatology for the CONUS (2000–2011). *27th Conf. on Severe Local Storms*, Madison, WI, Amer. Meteor. Soc., 146, https://ams.confex.com/ams/27SLS/webprogram/Paper255332.html.

——, ——, A. E. Reinhart, and T. M. Smith, 2018: A climatological study of hail occurrence using the MRMS MESH product. *29th Conf. on Severe Local Storms*, Stowe, VT, Amer. Meteor. Soc., 13A.1, https://ams.confex.com/ams/29SLS/webprogram/Paper348561.html.

Witt, A., M. D. Eilts, G. J. Stumpf, J. T. Johnson, E. D. Mitchell, and K. W. Thomas, 1998: An enhanced hail detection algorithm for the WSR-88D. *Wea. Forecasting*, **13**, 286–303, https://doi.org/10.1175/1520-0434(1998)013<0286:AEHDAF>2.0.CO;2.

Zhang, J., and Coauthors, 2016: Multi-Radar Multi-Sensor (MRMS) quantitative precipitation estimation: Initial operating capabilities. *Bull. Amer. Meteor. Soc.*, **97**, 621–638, https://doi.org/10.1175/BAMS-D-14-00174.1.